

## **Oxygenated VOC Detection Using SnO<sub>2</sub> Nanoparticles with Uniformly Dispersed Bi<sub>2</sub>O<sub>3</sub>**

Haoyue Yang<sup>1</sup>, Koichi Suematsu<sup>2\*</sup>, Felipe Hiroshi Mashiba<sup>1</sup>, Ken Watanabe<sup>2</sup>, and Kengo Shimano<sup>2\*</sup>

<sup>1</sup>*Interdisciplinary Graduate School of Engineering Sciences, Kyushu University, Kasuga, Fukuoka 816-8580, Japan*

<sup>2</sup>*Department of Advanced Materials Science and Engineering, Faculty of Engineering Sciences, Kyushu University, Kasuga, Fukuoka 816-8580, Japan*

### ***O<sub>2</sub>-TPD measurements***

Firstly, 0.2 g of sample were pressed and then ground to maintain the sizes of powders between 250 and 710  $\mu\text{m}$ . The obtained powders were put in reaction chamber and preheated at 550  $^{\circ}\text{C}$  for 2 h under synthetic air flow to refresh the surface. After cooled down to 100  $^{\circ}\text{C}$ , the samples were purged by helium (He) for 1.5 h. Finally, the sample was heated to 550  $^{\circ}\text{C}$  under He flow with a rate of 10  $^{\circ}\text{C}/\text{min}$ , as shown in Fig S1a. The desorbed signal from material surface during the heating period was detected by mass spectrometer. Herein, the mass spectrometer monitored the signal at mass number 32 was assigned to  $\text{O}_2$ .

### ***NH<sub>3</sub>-TPD measurements***

The procedure of  $\text{NH}_3$ -TPD was broadly similar with  $\text{O}_2$ -TPD. Before measurement, the pressed powders (250~710  $\mu\text{m}$ ) were preheated at 550  $^{\circ}\text{C}$  for 2 h and cooled down to 100  $^{\circ}\text{C}$  under air flow followed by purged using He for 1 h. Subsequently,  $\text{NH}_3/\text{He}$  flow was introduced for 30 min and then exposure to He flow for 30 min until the baseline was stable. Finally, the sample was heated to 550  $^{\circ}\text{C}$  under He flow with a rate of 10  $^{\circ}\text{C}/\text{min}$ , as shown in Fig S1b. The desorbed signal from material surface during the heating period was detected and recorded by TCD detector. Meanwhile, the signals at mass numbers 16 (the fragment of  $\text{NH}_3$  and  $\text{H}_2\text{O}$ ), 17 ( $\text{NH}_3$  and the fragment of  $\text{H}_2\text{O}$ ), 18 ( $\text{H}_2\text{O}$ ), 32 ( $\text{O}_2$ ), 14 ( $\text{N}_2$ ) and 28 ( $\text{N}_2$ ) were monitored by mass spectrometer.

### ***Catalytic combustion measurements***

Before measurement, the quantity of emitted gases was calibrated by neat nitrogen, oxygen, and standard gases. Firstly, 0.01g samples were pressed and then ground to maintain the sizes of powders between 250 and 710  $\mu\text{m}$ . Next, the obtained particles were put into the reaction chamber and preheated at 550  $^{\circ}\text{C}$  for 3 h under synthesis air flow. Subsequently, 100 ppm of ethanol/air or acetone/air was introduced when the reaction chamber was cooled to 350  $^{\circ}\text{C}$ , 300  $^{\circ}\text{C}$ , 250  $^{\circ}\text{C}$  and 200  $^{\circ}\text{C}$  with the rate of 5  $^{\circ}\text{C}/\text{min}$ . Finally, the consumption of ethanol or acetone and the productions ( $\text{C}_2\text{H}_4$ ,  $\text{CH}_3\text{CHO}$  and  $\text{CO}_2$ ) come from gas combustion at different temperatures were identified by GC analyzer.

### ***TPR measurements***

The desorption signals on  $\text{SnO}_2$  and 1Bi-L- $\text{SnO}_2$  surfaces after ethanol adsorption were investigated by TPR measurement. Firstly, 0.03g pretreated samples (250~710  $\mu\text{m}$ ) were put into reaction chamber and preheated at 550  $^{\circ}\text{C}$  for 3 h under  $\text{O}_2/\text{Ar}$  flow and then cooled to 200  $^{\circ}\text{C}$ , 250  $^{\circ}\text{C}$ , 300  $^{\circ}\text{C}$  and 350  $^{\circ}\text{C}$  with the rate of 5  $^{\circ}\text{C}/\text{min}$ , respectively. Subsequently, 100 ppm of ethanol/Ar was introduced for 1.5 h with the flow rate of 100  $\text{cm}^3 \cdot \text{min}^{-1}$  to adsorb ethanol molecules. Then the atmosphere was recovered to Ar flow containing 21% of  $\text{O}_2$  for 6 h. Finally, the powders were heated to 500  $^{\circ}\text{C}$  with the rate of 5  $^{\circ}\text{C}/\text{min}$  under  $\text{O}_2/\text{Ar}$  flow. The emission of gases during the heating period on material surfaces were analyzed by QMS detector at mass numbers 2 ( $\text{H}_2$ ), 17 ( $\text{H}_2\text{O}$ ), 44 (the fragment of  $\text{CH}_3\text{CHO}$  and  $\text{CO}_2$ ).

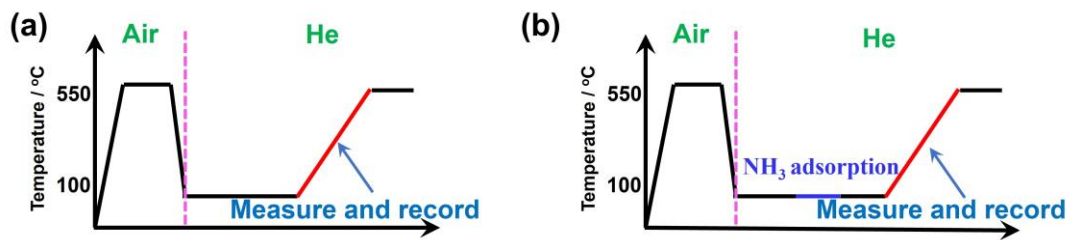


**Figure S1.** Explanation of operating processes during (a) O<sub>2</sub>-TPD and (b) NH<sub>3</sub>-TPD.

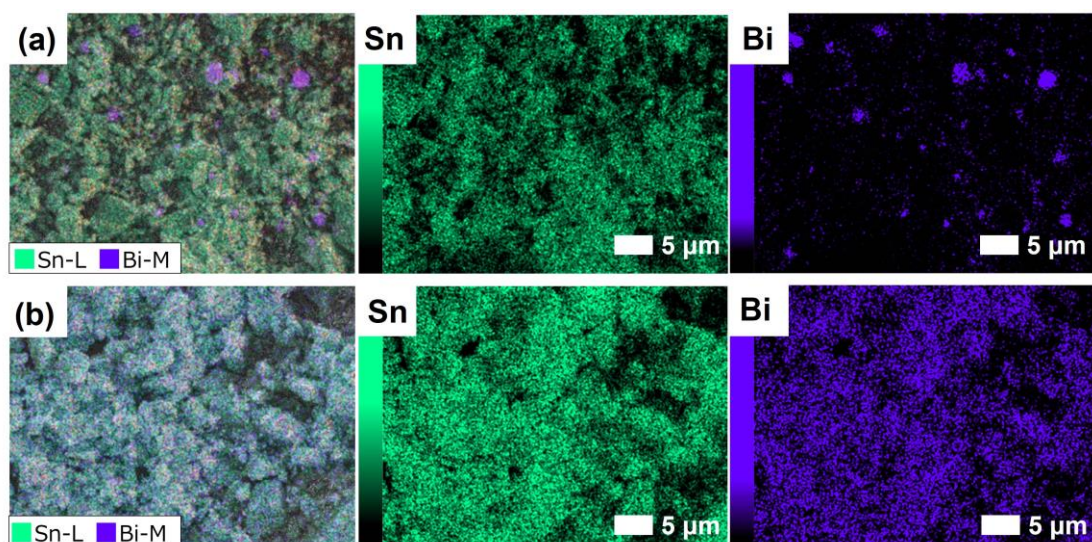


**Figure S2.** SEM-EDS mapping images of Sn and Bi elements for (a) 3Bi-M-SnO<sub>2</sub> and (b) 3Bi-L-SnO<sub>2</sub> samples.

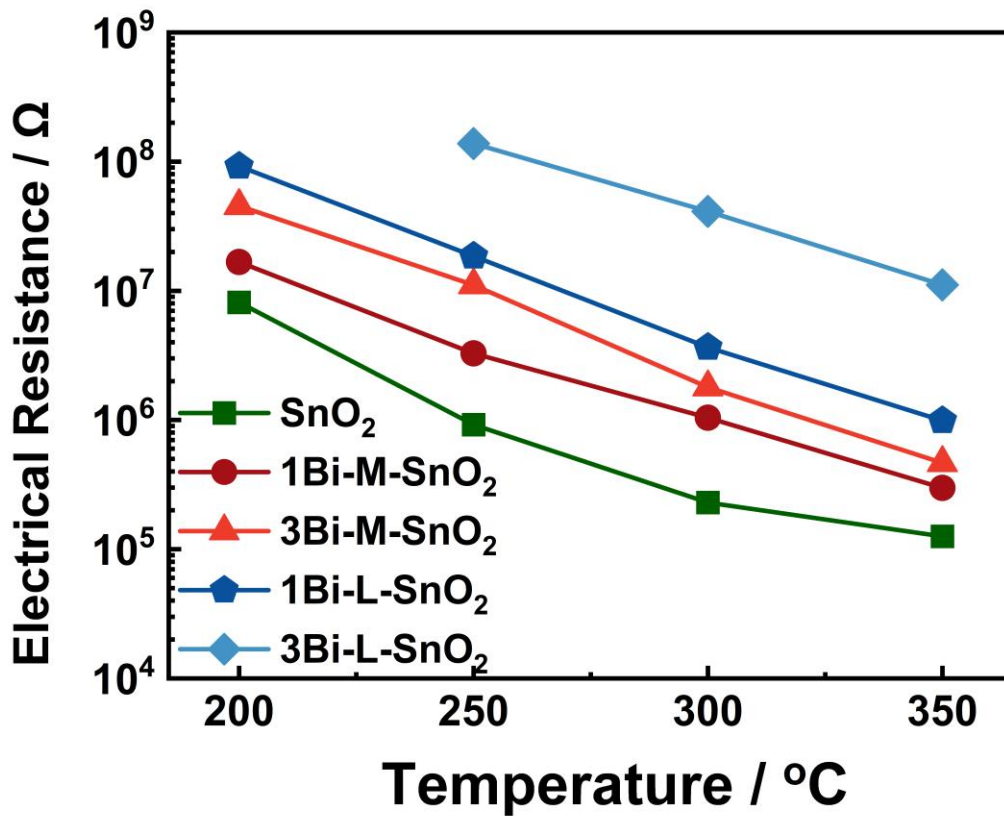


**Figure S3.** The electrical resistances in synthetic air of as-fabricated gas sensors at 200 °C, 250 °C, 300 °C and 350 °C.

Obviously, the  $R_a$  of all sensors was reduced with the increasing operating temperature, consistent with the semiconductor behavior. Moreover, both Bi<sub>2</sub>O<sub>3</sub>-mixing and Bi<sub>2</sub>O<sub>3</sub>-loading processes increased the  $R_a$  values of SnO<sub>2</sub>, and the  $R_a$  was enhanced with the rising amount of Bi<sub>2</sub>O<sub>3</sub> particles. Meanwhile, Bi<sub>2</sub>O<sub>3</sub>-loaded SnO<sub>2</sub> exhibited larger  $R_a$  than that of Bi<sub>2</sub>O<sub>3</sub>-mixed SnO<sub>2</sub> sensors, which could be associated the generation of potential barrier at Bi<sub>2</sub>O<sub>3</sub>/SnO<sub>2</sub> interfaces.

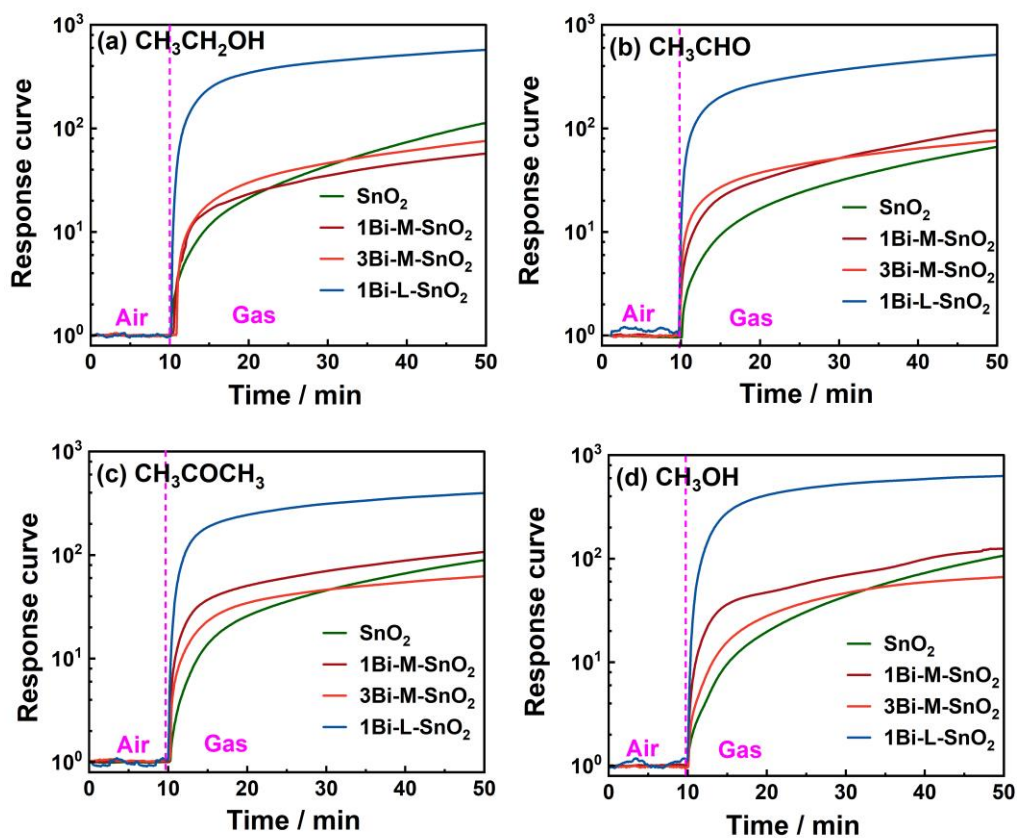


**Figure S4.** Dynamic time-dependence response curves of gas sensors to 5 ppm of (a)  $\text{CH}_3\text{CH}_2\text{OH}$ , (b)  $\text{CH}_3\text{CHO}$ , (c)  $\text{CH}_3\text{COCH}_3$ , (d)  $\text{CH}_3\text{OH}$  at 200 °C.

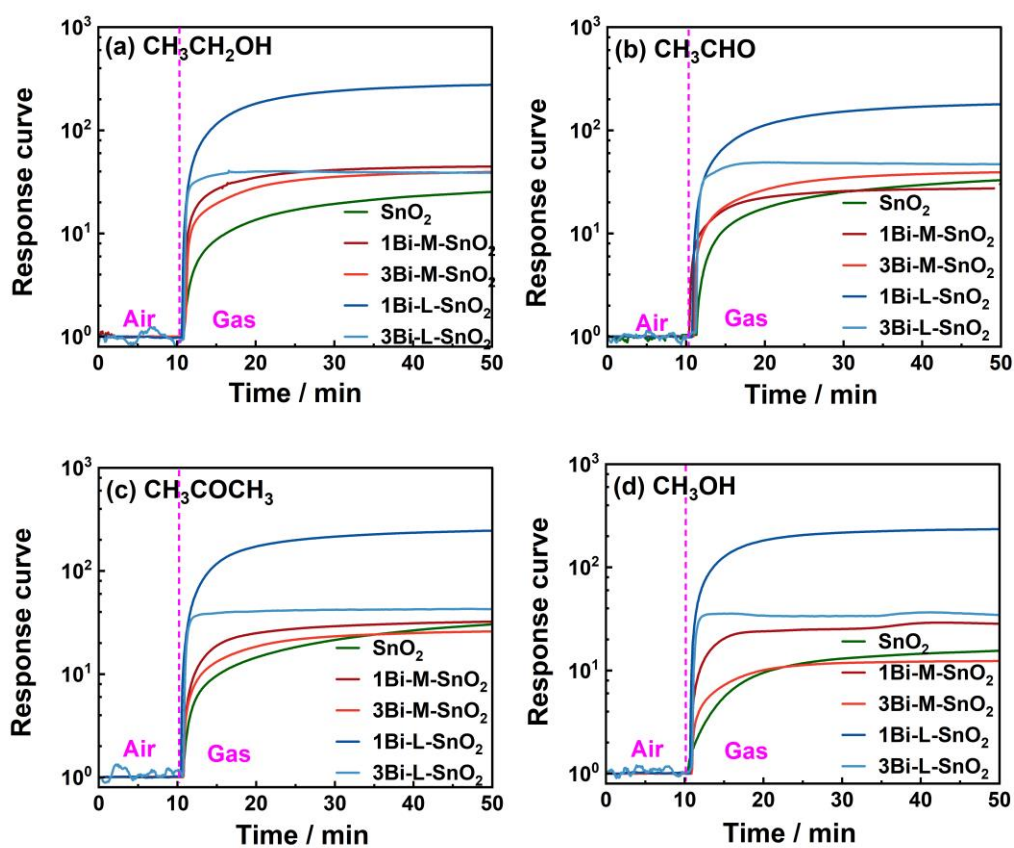


**Figure S5.** Dynamic time-dependence response curves of gas sensors to 5 ppm of (a)  $\text{CH}_3\text{CH}_2\text{OH}$ , (b)  $\text{CH}_3\text{CHO}$ , (c)  $\text{CH}_3\text{COCH}_3$ , (d)  $\text{CH}_3\text{OH}$  at 250 °C.

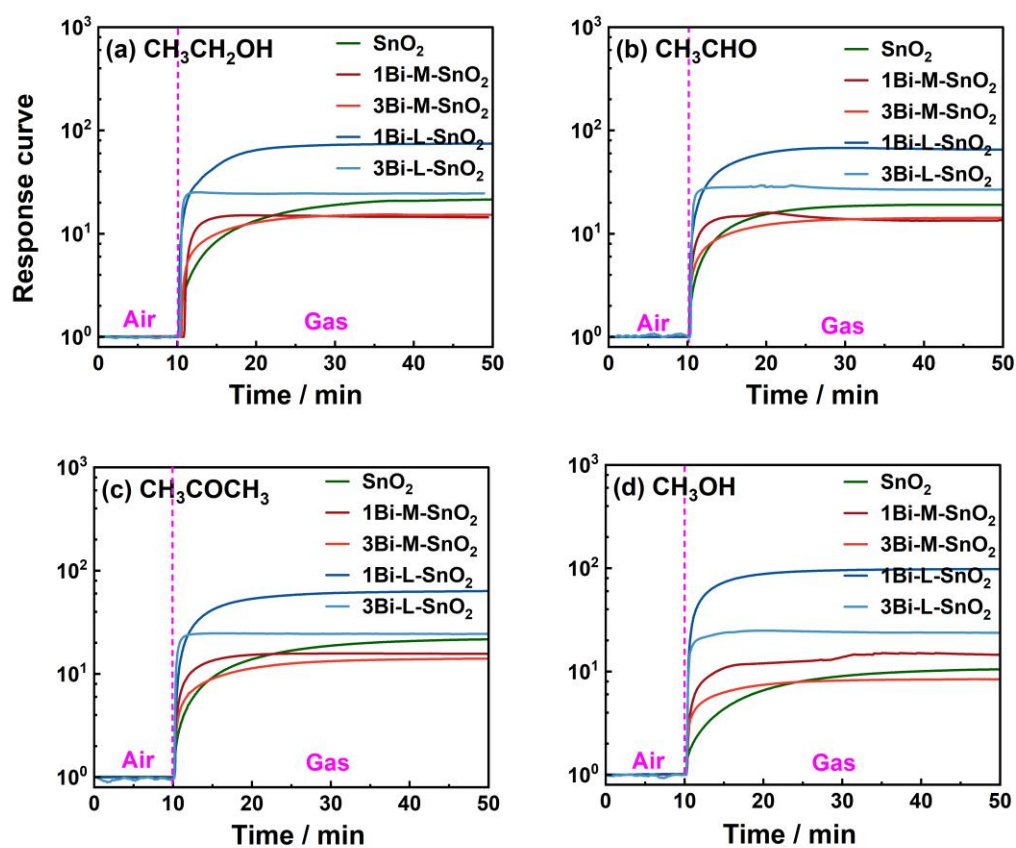


**Figure S6.** Dynamic time-dependence response curves of gas sensors to 5 ppm of (a)  $\text{CH}_3\text{CH}_2\text{OH}$ , (b)  $\text{CH}_3\text{CHO}$ , (c)  $\text{CH}_3\text{COCH}_3$ , (d)  $\text{CH}_3\text{OH}$  at 300 °C.

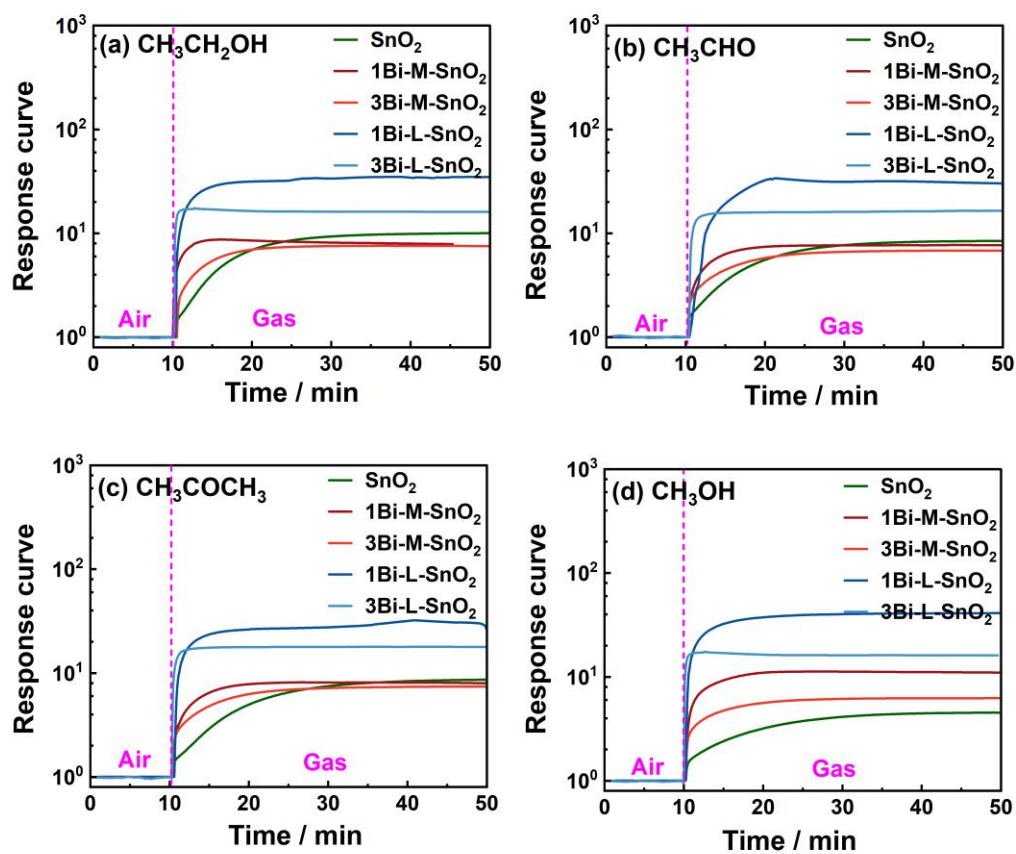


**Figure S7.** Dynamic time-dependence response curves of gas sensors to 5 ppm of (a)  $\text{CH}_3\text{CH}_2\text{OH}$ , (b)  $\text{CH}_3\text{CHO}$ , (c)  $\text{CH}_3\text{COCH}_3$ , (d)  $\text{CH}_3\text{OH}$  at 350 °C.

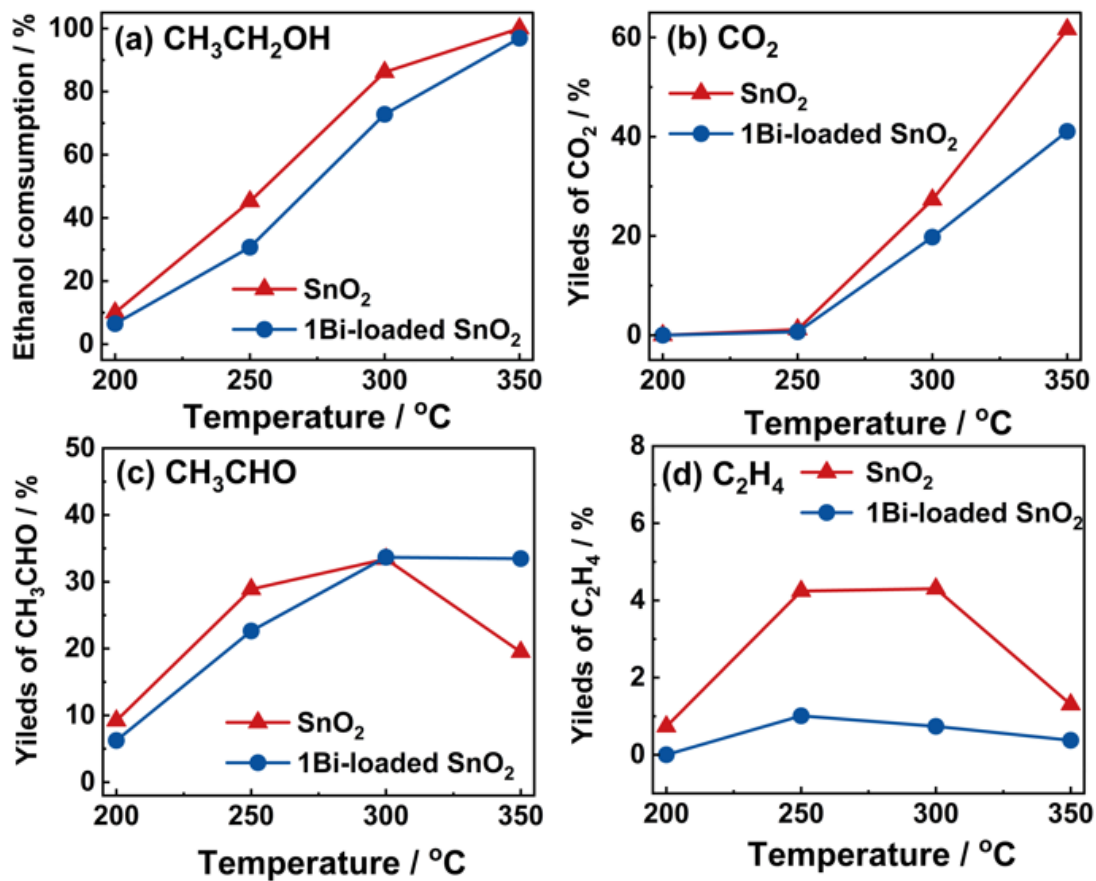


**Figure S8.** The temperature-dependence of (a) CH<sub>3</sub>CH<sub>2</sub>OH consumption, (b) CO<sub>2</sub>, (c) CH<sub>3</sub>CHO and (d) C<sub>2</sub>H<sub>4</sub> yields during ethanol combustion on the surfaces of SnO<sub>2</sub> and 1Bi-L-SnO<sub>2</sub> particles from 200 °C to 350 °C.

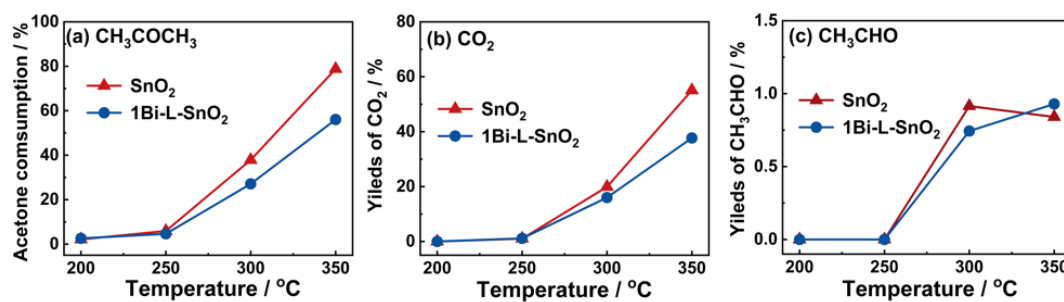


**Figure S9.** The temperature-dependence of (a) CH<sub>3</sub>COCH<sub>3</sub> consumption, (b) CO<sub>2</sub> and (c) CH<sub>3</sub>CHO yields during acetone combustion on the surfaces of SnO<sub>2</sub> and 1Bi-L-SnO<sub>2</sub> particles from 200 °C to 350 °C.

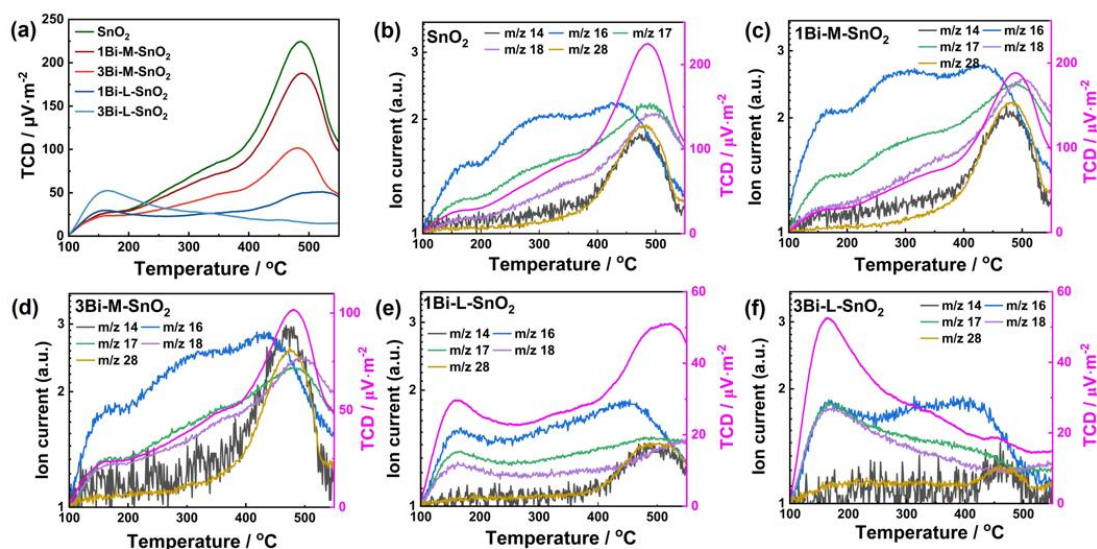


**Figure S10.** (a)  $\text{NH}_3$ -TPD profiles of as-prepared materials;  $\text{NH}_3$ -TPD combined with mass spectrometer spectra of (b)  $\text{SnO}_2$ , (c)  $1\text{Bi-M-SnO}_2$ , (d)  $3\text{Bi-M-SnO}_2$ , (e)  $1\text{Bi-L-SnO}_2$  and (f)  $3\text{Bi-L-SnO}_2$  materials.

Figure S10a showed the  $\text{NH}_3$ -TPD profiles of obtained materials. The desorption amounts recorded by TCD detector were divided their specific surface area. The peaks of  $\text{NH}_3$  on the surfaces of as-prepared materials could be divided to 100–200 °C and 200–550 °C. Obviously, the desorption amount of  $\text{NH}_3$  on  $\text{SnO}_2$  surface was gradually declined with the addition of  $\text{Bi}_2\text{O}_3$  particles. Interestingly,  $3\text{Bi-L-SnO}_2$  material showed slightly larger desorption amounts at 100–200 °C and extremely low desorption at higher temperature. The emitted gases from materials surfaces were further analyzed by mass spectrometer, as depicted in Figure S10b-f. At 100–400 °C, both  $m/z$  16 and  $m/z$  17 showed larger desorption peaks than  $m/z$  18, proving the emitted gases were mainly assigned to the desorption of  $\text{NH}_3$  molecules combined with a small amount of  $\text{H}_2\text{O}$ . Additionally, the distinct peaks at  $m/z$  14 and  $m/z$  28 during 400–550 °C were assigned to the generation of  $\text{N}_2$  caused by the decomposition of  $\text{NH}_3$ . And the comparable intensity between  $m/z$  17 and  $m/z$  18 suggested the production of  $\text{H}_2\text{O}$ . Therefore, the desorption peak at 100–200 °C was mainly ascribed to the desorption of molecular  $\text{NH}_3$  and  $\text{H}_2\text{O}$ , and the peak above 200 °C could be assigned to the physical and chemical adsorption of  $\text{NH}_3$  on the acid sites of  $\text{SnO}_2$ . In this context, the decreased desorption amounts during 200–550 °C on  $\text{Bi}_2\text{O}_3$ -mixed  $\text{SnO}_2$  and  $\text{Bi}_2\text{O}_3$ -loaded  $\text{SnO}_2$

materials indicated the reduced acidic sites of SnO<sub>2</sub> for NH<sub>3</sub> adsorption. Moreover, 3Bi-L-SnO<sub>2</sub> material showed distinct peak at m/z 18 during 100–200 °C, indicating the improved adsorption of molecular H<sub>2</sub>O. Consequently, the exposure of acid sites on the surface of SnO<sub>2</sub> was declined by the introduction of Bi<sub>2</sub>O<sub>3</sub> particles.

**Table S1.** Average crystallite size, BET and BJH results of SnO<sub>2</sub>, 1Bi-M-SnO<sub>2</sub>, 3Bi-M-SnO<sub>2</sub>, 1Bi-L-SnO<sub>2</sub>, 3Bi-L-SnO<sub>2</sub> materials.

Sample	Average crystallite size (nm) <sup>a</sup>	$S_{\text{BET}}$ (m <sup>2</sup> g <sup>-1</sup> ) <sup>b</sup>	$V_{\text{BJH}}$ (cm <sup>3</sup> g <sup>-1</sup> ) $\times 10^{-2}$ <sup>c</sup>
SnO <sub>2</sub>	12.03	13.7	4.16
1Bi-M-SnO <sub>2</sub>	10.93	15.7	4.51
3Bi-M-SnO <sub>2</sub>	13.23	17.5	4.89
1Bi-L-SnO <sub>2</sub>	10.95	17.7	4.52
3Bi-L-SnO <sub>2</sub>	11.25	17.8	4.78

<sup>a</sup> Average crystallite size: average crystallite size of SnO<sub>2</sub> calculated by Scherrer formula.

<sup>b</sup>  $S_{\text{BET}}$ : specific surface area calculated by BET method.

<sup>c</sup>  $V_{\text{BJH}}$ : pore volume calculated by BJH method.

**Table S2.** Response time of SnO<sub>2</sub> and Bi<sub>2</sub>O<sub>3</sub>-loaded sensors to 5 ppm of ethanol at 200–350 °C.

Sensor	200 °C	250 °C	300 °C	350 °C
SnO <sub>2</sub>	37.1 min	29.1 min	20.9 min	16.3 min
1Bi-L-SnO <sub>2</sub>	30.9 min	22.7 min	13.3 min	6.6 min
3Bi-L-SnO <sub>2</sub>	--	3.7 min	1.8 min	0.4 min